HHS Public Access

Author manuscript

J Neural Eng. Author manuscript; available in PMC 2020 December 17.

Published in final edited form as:

J Neural Eng. ; 17(1): 016016. doi:10.1088/1741-2552/ab51a5.

iEEGview: An Open-source Multifunction GUI-based Matlab Toolbox for Localization and Visualization of Human Intracranial Electrodes

Guangye Li[a,d], **Shize Jiang**[b], **Chen Chen**[a], **Peter Brunner**[c,d], **Zehan Wu**[b], **Gerwin Schalk**[c,d], **Liang Chen**[b], **Dingguo Zhang**[e,*]

[a]State Key Laboratory of Mechanical Systems and Vibrations, Institute of Robotics, Shanghai Jiao Tong University, Shanghai, China.

[b]Department of Neurosurgery of Huashan Hospital, Fudan University, Shanghai, China.

[c]Department of Neurology, Albany Medical College, Albany, NY, USA.

[d]National Center for Adaptive Neurotechnologies, Wadsworth Center, New York State Department of Health, Albany, NY, USA.

[e]Department of Electronic and Electrical Engineering, University of Bath, Bath, UK.

Abstract

Objective: The precise localization of intracranial electrodes is a fundamental step relevant to the analysis of intracranial electroencephalography (iEEG) recordings in various fields. With the increasing developments of the iEEG studies in human neuroscience, higher requirements have been posed on the localization process, resulting in urgent demands for more integrated, easy-operation and versatile tools for electrodes localization and visualization. Towards addressing this need, we develop an easy-to-use and multifunction toolbox called iEEGview that can be used for the localization and visualization of human intracranial electrodes.

Approach: iEEGview is written in Matlab scripts and implemented with a GUI. From the GUI, by taking only pre-implant MRI and post-implant CT images as input, users can directly run the full localization pipeline including brain segmentation, images co-registration, electrodes reconstruction, anatomical information identification, activation map generation and electrodes projection from native brain space into common brain space for group analysis. Additionally, iEEGview implements methods for brain shift correction, visual location inspection on MRI slices and computation of certainty index in anatomical label assignment.

Main Results: All the introduced functions of iEEGview work reliably and successfully, which are tested by images from 28 human subjects implanted with depth and/or subdural electrodes.

Significance: iEEGview is the first public Matlab GUI based software for intracranial electrode localization and visualization that hold integrated capabilities together within one pipeline. iEEGview promotes convenience and efficiency for the localization process, provides rich

*Corresponding author. d.zhang@bath.ac.uk (DG. Zhang).

localization information for further analysis and offers solutions for addressing raised technical challenges. Therefore, it can serve as a useful tool in facilitating iEEG studies.

Keywords

Localization; Visualization; iEEG; SEEG; ECoG; Matlab toolbox; Electrodes

1. Introduction

For patients with medically intractable epilepsy, intracranial electroencephalography (iEEG) has been widely applied in the exploration of epileptogenic zone and the identification of eloquent cortex (Behrens et al., 1994; Lachaux et al., 2003). In terms of the types of implanted intracranial electrodes, iEEG mainly includes two modalities. One is known as electrocorticography (ECoG), which implants subdural grid electrodes or strip electrodes and has been a most common technique in the past decades (Crone et al., 2006). The other modality, named as stereo-encephalography (SEEG), using depth electrodes containing multiple contacts to acquire intracranial data, which has become increasingly prevalent in clinical practice (Bartolomei et al., 2018; Ayoubian et al., 2010; Britton, 2018; Cardinale et al., 2016; Landre et al., 2018). Owing to the merits of high spatiotemporal resolution and simultaneous recordings across different cortical areas or subcortical structures, iEEG has not only been used for clinical practice but has also become an invaluable tool for neuroscientific research and translational applications (Parvizi and Kastner, 2018; Ter Wal et al., 2018; Leuthardt et al., 2004).

Notably, accurate localization of intracranial electrodes plays a critical role in guaranteeing the precision of iEEG-related analyses (Taimouri et al., 2014; Gonzalez-Martinez et al., 2014; Pieters et al., 2013). In clinical practice, the accurate information for both the relative position and anatomical location of each iEEG electrode in relationship to brain, are extremely important in either the assessment of epileptogenic zone resection (Taimouri et al., 2014; Koessler et al., 2010; Trebuchon and Chauvel, 2016) or the mapping of functional cortex (Brunner et al., 2009; Swift et al., 2018). While neuroscientific research needs the anatomical label of each iEEG electrode for functional analyses within the individual brain (Li et al., 2018a; Coon and Schalk, 2016; Schalk et al., 2017a), or the normalized electrode positions across different subjects for group analyses in the standard brain (Arnal et al., 2019; Betzel et al., 2019; Avanzini et al., 2016; Schalk et al., 2017b; Posner et al., 2014; Nourski et al., 2018). In translation applications (e.g., brain-machine interface), identifying anatomical location of activated electrodes and visualizing the overall subsequent cortical activation map is essential for a better understanding of brain functions during a certain task (Kubanek et al., 2009; Schalk et al., 2007; Li et al., 2017; Murphy et al., 2016). In summary, to meet the various requirements from existing iEEG applications, the localization process should provide at least four functions, including - 1) localizing the 3D coordinates of iEEG electrodes within each individual brain; 2) identifying the anatomical information for iEEG electrodes for that brain; 3) visualizing brain activation using iEEG recordings; 4) mapping electrodes from different individual subjects into a common standard brain.

Till now, different methods have been developed to locate implanted electrodes. Some methods use solely MRI images to identify electrode locations (Yang et al., 2012; Kovalev et al., 2005), however, the post-implant MRI requires special type of electrodes and also has the potential risks of electrode induction heating (Bhavaraju et al., 2002). Another method to localize the electrode is solely through X-ray images (Miller et al., 2007), although it is time-saving and comparatively safe, this approach lacks the individual anatomical information. Therefore, the most commonly used method is combining pre-implant MRI and post-implant CT images to obtain greater localization accuracy (van Rooijen et al., 2013). Using co-registered CT and MRI images, although some public software have succeed in reconstructing the iEEG electrode positions (Taimouri et al., 2014; Dykstra et al., 2012; Blenkmann et al., 2017), they are short of some important functions as required (e.g., visualizing brain activation, identifying anatomical information for each electrode and/or projecting into a standard brain). Meanwhile, some other well-developed software have only been validated for either the localization of depth (Medina Villalon et al., 2018; Narizzano et al., 2017; Arnulfo et al., 2015b; Princich et al., 2013) or subdural (Azarion et al., 2014; Kovalev et al., 2005; Branco et al., 2018a,b; Hermes et al., 2010) electrodes, where they are not adequate for the potential clinical needs when the combination of these two type of electrodes are implanted (Surbeck et al., 2011; Enatsu et al., 2014). More recently, a toolbox, providing enriched functions and being used for localizing both depth and subdural electrodes, has been introduced (Groppe et al., 2017), but in one aspect, it lacks of providing enough important anatomical information for each electrode (e.g., the degree of confidence that a depth electrode contact can be assigned to a brain region); in other aspect, it still needs additional efforts on manual operation across multiple third-party software packages, which may increase the burden for inexperienced users during operation.

To address above issues, by incorporating previous developed software (Kubanek and Schalk, 2015; Li et al., 2018b), we provide a fully upgraded toolbox package that can localize and visualize depth (SEEG) and subdural (ECoG) electrodes (or the combination) with multiple functions in a semi-automatic way in this work. This toolbox integrates all dependent software in one Matlab interface using command lines. Besides, it is GUI (Graph User Interface) based and featured with rich choices, which is time-saving and user-friendly. With just simple inputs from the user which is guided by the GUI, the toolbox performs the full pipeline (from images to all features as mentioned above).

2. Electrodes Reconstruction

iEEGview is developed using Matlab (Mathwork, Natick, MA), and it also uses some Bash scripts for the automatic interaction with Freesurfer (http://surfer.nmr.mgh.harvard.edu), where Freesurfer is used for the basic image processing, brain reconstruction and electrodes profile extraction during the electrodes localization process, and Freesurfer-produced results are used across the full localization pipeline. The entire toolbox is required to run under a Mac OS system and has been tested with the Mac OS X system and Matlab version (R2017b, v9.3) or higher. Images from 28 human subjects are used for testing the toolbox (3158 depth electrode contacts and 598 subdural electrodes are implanted in total, all subjects gave the informed consent), where 22 subjects implant depth electrodes (Subject 1–

22), 5 subjects are with subdural electrodes (Subject 23–27), 1 subject (Subject 28, also known as Subject UCI29) implants both depth and subdural electrodes (Stolk et al., 2018).

The electrode localization process is shown in Fig. 1. In detail, as the first step of electrode localization, iEEGview takes pre-implant T1-weighted MRI images as inputs and then reconstructs the individual brain model by invoking the Freesurfer automatically using Bash scripts (Fig. 1A). This process first transforms the input MRI brain volume into a Freesurfer right-anterior-superior (RAS) coordinates space, then runs the brain volume reconstruction. The reconstruction produces not only the pial and white matter surfaces from both hemispheres (Fig. 1B), but also the cortical parcellation (Desikan et al., 2006; Destrieux et al., 2009; Fischl, 2004) and subcortical segmentation (Fischl et al., 2002) results. These results are saved by the toolbox and used for the following localization pipeline.

At the second step, the toolbox aligns post-implant CT (Fig. 1D) with pre-implant MRI automatically using the built-in Matlab functions (spm_coreg, spm_reslice) from SPM 12 (Penny et al., 2011). More specifically, the coregistration process is implemented through an affine transformation with six degree of freedom based on the maximization of normalized mutual information (Jenkinson and Smith, 2001; Studholme et al., 1998). This method has shown its good performance for the coregistration of CT and MR images (Azarion et al., 2014; Hermes et al., 2010; Studholme et al., 1998). After this, the toolbox automatically displays the coregistered volumes in Freesurfer. This step enables the user to visually check the coregistration results and also extract the electrode information including surface and location of implanted electrodes by thresholding the coregistered CT images (Fig. 1E, see also Supplementary Materials). Following this step, the toolbox then provides a GUI for users to manually label‡ each of the derived electrodes in 3D space (visualized by small number of vertices and triangles in Matlab, Fig. 1E). For the subdural electrodes, the 3D coordinates of all the electrodes, that in the same coordinate space with the individual brain model, are automatically obtained after labelling (Fig. 1F). Notably, such 3D space electrode visualization also provides users additional advantages towards the traditional 2D space visualization (Hermes et al., 2010; Dykstra et al., 2012) in the detection of overlapping subdural electrode implants (Branco et al., 2018a). While for depth electrodes, considering the facts that a large number of depth electrode contacts are generally used and also the size of each contact is much smaller than typical subdural electrodes, this process will thus be difficult and time-consuming. Therefore, to make the electrode localization process more efficient, iEEGview only requires four randomly spaced points to be selected from each extracted electrode shaft surface to conduct a line fitting process using the least square method (Moré, 1978; Li et al., 2018b), where the first point should be selected from the tip of each electrode shaft (deep brain layer). Then with the user solely inputting the number of contacts along each electrode shaft from the GUI of iEEGview, the 3D coordinates of all the depth contacts can be automatically generated.

Notably, brain shift occurs due to various factors that include brain swelling, drainage of cerebro-spinal fluid, surgical intervention, and a deformation following gravity and electrodes implant (Hastreiter et al., 2004; Dalal et al., 2008). Roberts et al. reported a brain

‡feedback on the electrodes that have been labelled is provided in the GUI for the convenience of operation

displacement of 1 cm on average during craniotomy (Roberts et al., 1998). Therefore, to guarantee a higher localization accuracy, brain shift correction is generally a necessary step in electrode localization when a craniotomy is made. Using the methods introduced in previous work (Kubanek and Schalk, 2015; Yang et al., 2012; Blenkmann et al., 2017), we provide brain shift correction functions within the iEEGview toolbox for either when subdural electrodes are implanted solely or depth electrodes are implanted along with subdural electrodes where a craniotomy is required. Specifically, for subdural electrodes, a smoothed surface (Fig. 1C) that deprives of sulci from the reconstructed pial surface is first built by the toolbox using the morphological closing algorithm for the projection purpose (Yang et al., 2012; Schaer et al., 2008). Before the projection, since such brain surface still consists of a large number of vertices and triangles, which is computationally expensive, we then produce a simplified version of the smoothed brain surface by reducing the vertices and triangles to speed up the calculation for both hemispheres. After this, iEEGview projects each electrode ($P_k(x,y,z)$) onto a coordinate ($P'_k(x,y,z)$) of the simplified brain surface. In brief, the procedure firstly finds all vertices $V_i(x,y,z),(i = 1...N)$ of the simplified brain surface within a predefined radius (e.g., 25 mm by default) from the electrode ($P_k(x,y,z)$). Then, the normal vectors of all the triangles touching these vertices are averaged ($\overrightarrow{A}(x,y,z)$). Finally, the intersection between the electrode ($P_k(x,y,z)$) and simplified brain surface following the averaged normal vector ($\overrightarrow{A}(x,y,z)$) is identified as a projection point ($P'_k(x,y,z)$) Kubanek and Schalk, 2015). This projection point ($P'_k(x,y,z)$) is used as the final coordinates for each subdural electrode ($P_k(x,y,z)$) after brain shift correction (Fig. 1H and J).

For the scenario of depth and subdural electrodes are implanted simultaneously, we additionally correct the brain shift for depth electrodes. This process is implemented by using a weighted displacement field function based on the subdural electrodes' brain shift correction results and the distance to uncorrected subdural electrodes (Blenkmann et al., 2017). In detail, the weighted displacement field function (Eq. 1) translates the inputs using two gaussian kernel based functions, where one (Eq. 2) is used to compute the displacement field (Taimouri et al., 2014); the other one (Eq. 3) weights the displacement field with distance considering the fact that depth electrodes that located in deeper layer of the brain are less affected by the brain deformation than the ones close to the brain surface (Fig. 1G and I).

$$D_j = \frac{\sum_{k=1}^{K} w_{jk} w'_{jk} D_k}{\sum_{k=1}^{K} w_{jk}} \tag{1}$$

$$w_{jk} = e^{-\frac{\|P_j - P_k\|}{\sigma_R^2}} \tag{2}$$

$$w'_{jk} = e^{-\frac{\|P_j - P_k\|}{\sigma_D^2}} \tag{3}$$

where P_j and P_k are the coordinates of the uncorrected depth contact j and subdural electrode k; D_k is the projection vector for subdural electrode k, ($k = 1...K$), $D_k = P'_k - P_k$; and σ_D are regularization parameters and are set as 5 mm and 30 mm within the toolbox respectively. The final coordinates P'_j for the depth contact P_j after brain shift correction is then obtained as the $P'_j = P_j + D_j$.

One of the brain shift correction examples for both subdural and depth electrodes is shown in Fig. 1G–J. We run this process for each of six applicable subjects, the averaged brain shift correction value is 3.71±0.13 (mean±s.e) mm for subdural electrodes (n=568) and 0.89±0.08 (mean±s.e) mm for depth electrode contacts (n=32).

This entire brain and electrodes reconstruction process for each subject typically takes about 8–24 hours of computing time for brain segmentation from Freesurfer and 30–60 minutes of operation time (i.e., for localization of all electrodes) for an experienced user.

3. Anatomical Information Identification

For intracranial electrodes based analysis, another essential requirement is to identify the anatomical location for each electrode. iEEGview automatically identifies anatomical label for each intracranial electrode (i.e., depth and subdural electrodes) (Fig. 2). This identification uses the brain segmentation results from the Freesurfer (see Sec. 2), which yields a range of different cortical areas and also subcortical structures such as left and right cerebral white matter, caudate, putamen, thalamus, hippocampus, amygdala and other components (Fischl et al., 2002). The segmentation results are saved in the format of entire brain volume which is with a size of 256×256×256 under a voxelbased column-row-slice (CRS) coordinate system. Within the brain volume, each voxel is 1×1×1 mm^3 and carries an anatomical label (Fig. 3A). For depth electrodes (e.g., SEEG), to enhance precision in anatomical label assignment, we use a shape-based volumetric classification method instead of using only the centroid of each contact. More specifically, we build an augmented contact by adding a 0.5 mm tolerance into the original contact (e.g., 2 mm length, 0.8 mm diameter) in both length and radius direction and then project this cylinder into the target segmented brain volume. Then we cluster all the voxels that touch with this cylinder, the anatomical location of the contact is classified into the group that has maximum number of same voxels within this cluster (Fig. 2A–B). While for subdural electrodes, the anatomical location for each electrode is identified as the anatomical name of maximum same labelled vertex, among the vertices surrounding (e.g., within 5 mm) the point where the computed electrode is located after brain shift correction (Fig. 2C–D). Additionally, to fulfill the potential multiple needs, iEEGview provides three atlases (Desikan-Killiany (Desikan et al., 2006), Destrieux (Destrieux et al., 2009; Fischl, 2004), DKT40 (Klein and Tourville, 2012)) for the usage of cortical areas identification. Moreover, to meet the possible needs on the white matter related analysis using depth electrode recordings, the toolbox also provides the function of identifying the anatomical label for the depth electrode contact that located in the superficial white matter tracts (white matter that are closest to divided cortical areas, e.g., pre/post-central white matter, up to 36 zones), where the white matter segmentation results from Freesurfer are used (Fig. 2J–L).

Considering that the depth electrode contact is typically long cylinder shape, therefore, each contact may span two or more different structures (e.g., gray matter and white matter), causing uncertainties on its anatomical location. While some subcortical studies (e.g., white matter) that may need to find out the contacts that are located in white matter for sure so as to make the corresponding subcortical analysis robust. For this purpose, iEEGview provides the automatic calculation of an index called proximal tissue density (PTD) (Mercier et al., 2017), which reflects the degree of confidence that an electrode can be assigned to a particular anatomical region. In details, for each augmented depth contact, we calculate the PTD following the equation (Eq. 4). A schematic drawing of PTD algorithm is shown in Fig. 3A. Using this method, we computed the PTD value across 23 subjects implanting depth electrodes. The distribution of different PTD value bins is shown in Fig. 3B. The results demonstrate that 19.1% of the depth contacts are totally embedded by gray matter, and 20.3% by white matter, leaving approximately 60% of depth contacts surrounded by both gray matter and white matter. These results also emphasize the importance of taking the uncertainty of anatomical labelling into consideration for each depth contact when conducting analysis in relationship to anatomy, where the introduced PTD index is a feasible solution to this. To enrich the options for the users, we additionally provide the computation of PTD value using the method introduced in (Mercier et al., 2017), which identifies the number of gray and white matter voxels within a 3×3×3 mm^3 volume surrounding the centroid of each depth contact (Eq. 4), where the PTD values computed using both methods are similar (Mercier et al., 2017).

$$PTD = (V_g - V_w)/(V_g + V_w) \tag{4}$$

where V_g and V_w are the identified number of gray matter and white matter voxels that completely or partially overlapped with the contact.

Even though automatically identifying the anatomical location is time saving, manual inspection of the anatomical location for each electrode or depth contact is still essential for some experienced users to obtain a higher localization accuracy. Moreover, manual checking also provides more details for the anatomical locations. To fulfill such needs, iEEGview offers the function for manually visual inspection as well. Using this function, the toolbox provides three different views (sagittal, coronal and axial view) of both gray scale MRI images and colored segmented brain images. Within each view, the users can visually check the location of each electrode (or depth contact) just by simply adjusting the slices of each view (Fig. 2F–H and J–L). Also, a 3D view of the entire brain and electrodes with a cursor is displayed to show the present slice position for reference (Fig. 2I). The automatically identified anatomical label for the electrodes located in the present MRI slices are shown as well for comparison purpose (Fig. 2E, see Supplementary Materials for more details about the manipulation).

4. Activation Map Visualization

Visualization of brain topographies associated with neural activity on the cortical surface plays an important role in vividly and directly expressing neural information, we termed it as

the activation map here. By giving the activation value, iEEGview can plot the activation map automatically. The activation value can be either a component related with neural activation status (e.g., gamma/alpha activity (de Pesters et al., 2016; Miller et al., 2010)) or a statistical indicator of neural recordings (e.g., −log(p) value (Schalk et al., 2007; Li et al., 2017)). In detail, this process treats each subdural electrode or depth electrode contact as a neural source, where the source is of the same coordinates with the electrode or contact itself after brain shift correction (Fig. 4A and C, See Sec. 2). iEEGview then computes the effective activation value of each vertex surrounding the electrode (Kubanek and Schalk, 2015). This process is made up with four steps: 1) The process first finds all vertices that under a certain distance range from the electrode; 2) For each identified vertex, the toolbox provides two different applicable kernel functions (Eq.5–6 and Eq.7–8) to calculate the activation factor (K_{act}, [0, 1]) based on the distance from the vertex to the electrode considering the potential attenuation effect from a neural source; 3) Since one vertex may be affected by multiple sources and hence generating more than one activation factors for each vertex after step 2, the toolbox then implements a normalization procedure to prevent cumulative effects on following activation value calculation due to difference on number of sources (i.e., dividing K_{act} from each source by the summation of K_{act} from all available sources in each vertex). The activation value of each vertex is computed by multiplying each normalized activation factor with the activation value from each electrode that entered by the user; 4) Finally, the activation map is rendered using the averaged activation value that carried by each vertex.

Linear Kernel:

$$K_{act}(d) = f_l(d, D) \tag{5}$$

$$f_l(d, D) = \begin{cases} 0; & (d >= D) \\ 1 - \frac{d}{D}; & (d < D) \end{cases} \tag{6}$$

Gaussian Kernel:

$$K_{act}(d) = f_g(d, D) \tag{7}$$

$$f_g(d, D) = e^{-\frac{d^2}{2D^2}}; \tag{8}$$

where d means the distance from each subdural electrode or depth contact to each cortical vertex within range R (R adjustable, 10 and 15 mm for subdural and depth electrodes by default in the toolbox), D is the cutoff distance that is used to adjust the attenuation effect for the activation map (D adjustable, 10 mm by default in the toolbox).

Within the iEEGview, the toolbox provides users the function of freely choosing and setting the parameters based on the personal needs. An example of rendered activation map for depth and subdural electrodes are shown in Fig. 4B and D.

5. Standard Brain Mapping

Group level analysis and visualization is always essential in the iEEG based researches in uncovering the universal phenomena underlying the recorded neural activities when studying from large number of subjects. To address the needs for group analysis and visualization, iEEGview provides the function of mapping the intracranial electrodes to a standard brain model across multiple subjects (Fig. 5).

Specifically, two representative standard brain templates for this function are utilized in the toolbox, one is a Montreal Neurological Institute (MNI) brain template (Fig. 5A–H), this brain model is first constructed with high resolution MRI images from single subject and thus featured with rich cortical surface information (known as “Colin27”) (Holmes et al., 1998), and then the template is normalized to MNI152 space in this work (Evans et al., 2012; Mazziotta et al., 1995); the other one is the averaged brain from Freesurfer (known as “FSAverage”, Fig. 5I–P, MNI305 space), this brain template is made from the spherical alignment of 40 subjects and featured with less cortical surface areas because each individual’s brain get smoothed out during the group average process (Fischl et al., 1999).

For subdural electrodes, iEEGview provides two different methods for the mapping of electrodes into the common brain space (Stolk et al., 2018), where one is volume-based registration (Ashburner and Friston, 1999; Fischl et al., 1999; Conner et al., 2014) and the other one is surface-based registration (Dykstra et al., 2012). These two different methods are implemented on two brain templates separately. For the volume-based registration method, iEEGview takes the MNI brain template. Specifically, this process first normalizes (spm_normalise) the individual brain model to a standard MNI brain template (Mazziotta et al., 1995), generating consequently the volume registration correspondence between these two brain models, which is represented by a series of nonlinear transformation matrices. Then the process warps all the electrodes from the native brain space into the common MNI brain space (MNI152) using derived nonlinear transformation parameters; for surface-based registration method, the iEEGview uses Freesurfer average brain template (FSAverage). Briefly, for each individual brain pial surface, a sphere-version surface is first gyrally aligned to the average brain pial surface (Freesurfer), where such spherical surface has a one-to-one vertex correspondence with pail surface. Then the toolbox obtains a projection point for each electrode by finding the closest vertex on the pial surface of individual brain. After this, each projection point on the individual spherical surface is assigned to the nearest vertex on the average brain spherical surface, where the corresponding coordinates of this assigned vertex on Freesurfer average brain pial surface (FSAverage) is identified as the mapping point finally in the common brain space. While for the depth electrodes, iEEGview also provides two different ways of mapping (Stolk et al., 2018; Li et al., 2018b) on the introduced two brain templates respectively as well, one is volume-based registration, this process maps each depth electrode contact into the common MNI brain space (MNI152) nonlinearly, which is the same with subdural electrodes; the other approach utilizes linear space transformation, which directly projects each depth electrode contact from native brain space to another common brain space (MNI305) where the Freesurfer average brain template is located using an affine transformation (Collins et al., 1994).

Figure 5 presents the results of introduced standard brain mapping functions using iEEGview for depth and subdural electrodes, where 3158 depth contacts from 23 subjects (Subject 1–22 and 28) and 568 subdural electrodes from 6 subjects (Subject 23–27 and 28) are used. Furthermore, after the mapping, by treating the standard brain as an individual model, iEEGview can compute the group-level activation map directly on the standard brain model using the introduced method (Sec. 2 and 4) across multiple subjects (Fig. 5A and I).

6. Discussion

With the increasing importance of iEEG related research, public software packages that can address the technical challenges posed in this work are in urgent demands. We here introduce the iEEGview toolbox for the research community that meets the criteria of accurate localization of either depth/subdural electrodes or the both. In particular, a GUI with rich choices is developed for iEEGview to implement all the required functions (See Supplementary Materials), making the operation from users easy and time-saving. From the GUI, the users can directly run the full pipeline through the listed menu, starting from pre-implant MRI and post-implant CT images, to the segmentation of brain, the coregistration of images and the acquisition of 3D coordinates of all electrodes; to the identification of each electrode's corresponding anatomical information and visual inspection of each localized electrode on the original MRI slices; to the projection of electrodes from native brain space into a common brain space across multiple subjects; and to the computation and visualization of activation map on the rendered brain surface in both native brain space and common brain space. Additionally, the GUI presents together 2D and 3D views of the computing results on the rendered brain to facilitate the understanding of electrodes information in relationship to brain anatomy. Importantly, all of these introduced functions have been validated successfully under a large number of subjects (n=28).

Brain shift correction for subdural and depth electrodes is implemented in the iEEGview when subdural electrodes are implanted solely or implanting together with depth electrodes, where a craniotomy is made. Mean correction distance achieved from multiple subjects using methods proposed in this work (Sec. 2) is comparable with previous studies (Blenkmann et al., 2017; Branco et al., 2018a; Dykstra et al., 2012; Hermes et al., 2010), certifying the localization accuracy of current toolbox. While when depth electrodes are implanted alone, we do not implement such correction because the brain shift caused in stereotactic surgeries is generally small (Elias et al., 2007; Sweet et al., 2013). This is the same with other studies (Medina Villalon et al., 2018; Narizzano et al., 2017; Arnulfo et al., 2015b).

Notably, iEEG is extensively adopted for studying the human cortex layer during the past decades (Schalk et al., 2007; Swift et al., 2018; Coon et al., 2016). Subcortical structures, such as white matter, which remains largely ignored and unknown. Meanwhile, depth electrodes have the huge potentials to be taken as a unique tool to investigate signals that recorded under the gray matter with high temporal resolution (Parvizi and Kastner, 2018). However, these studies rely on the accurate identification on the anatomical locations for each depth electrode contact. iEEGview has the capability of fulfill such needs in several aspects. First, iEEGview toolbox can identify the anatomical information for each depth

electrode contact and provide various atlases for users to choose from. Second, for the channels that located in superficial white matter fiber tracts (Guevara et al., 2017), iEEGview can also provide the label of which cortical regions of interest (ROIs) that these white matter channels are adjacent to based on the Freesurfer white matter segmentation results (Salat et al., 2009). Third, the toolbox provides the measure on the degree of confidence that an electrode can be assigned to a particular anatomical region (e.g., PTD), which is essential in the evaluation of subcortical structures (Mercier et al., 2017; Arnulfo et al., 2015a). Just recently, a toolbox developed for estimating probability of intracranial electrodes being assigned to specific neuroanatomical atlas using a different approach is reported (Behncke et al., 2019), indicating again the importance of offering probability of anatomical label assignment for each electrode in iEEG studies.

In addition to above features, the toolbox provides the techniques for mapping intracranial electrodes into common brain space using volumetric and/or surface-based registration methods implementing on two most commonly used brain templates. In detail, both volumetric (Conner et al., 2014; Schalk et al., 2017b) and surface-based (Dykstra et al., 2012; Groppe et al., 2017) mapping approaches are offered for subdural electrodes; besides, for the depth electrodes, the toolbox also provides volumetric transformation (Blenkmann et al., 2017; Sani et al., 2018) and linear space transformation (Li et al., 2018a; Groppe et al., 2017) methods for the mapping. Moreover, iEEGview integrates such mapping techniques for sudural and depth electrodes on the same brain template, and thus, either of these two templates can accommodate both subdural and depth electrodes together. This design may benefit the users from several aspects: first, this could enable the users to analyze directly across different electrodes types within one standard brain model without extra transforming efforts between spaces; second, it could also provide the possibility to make separate cross-modality comparison (e.g., fMRI results) for a comprehensive brain physiology studies; third, providing two brain templates could also meet potential various needs on group analysis in a larger extent. Even though we have introduced a series of intersubject mapping techniques, notably, we do not compare the mapping accuracy among the proposed methods in this work since the ability to cross-register functional intracranial recordings across various individuals has been proven difficult and thus will be further investigated (Wu et al., 2018).

Even though iEEGview has provided a set of essential functions for the localizing and visualizing intracranial electrodes, there are still some shortcomings for the current software package. One is that, we used a manual or semi-automatic way (e.g., label each of the subdural electrodes or label four points along each depth electrode shaft), instead of a fully automatic detection method, to obtain the coordinates of all electrodes by thresholding the CT images after coregistration. Comparing with the automatic approach (Blenkmann et al., 2017), current method we have taken in the iEEGview will be helpful in preventing from mistaken detection when the contrast of CT images between the electrodes and brain tissues is not high enough, however, automatic detection will mostly be much more time-saving. Therefore, the automatic detection algorithm on both depth and subdural electrodes should be developed and provided as an option for users in the next stage.

Additionally, as a measure of cortical activities, we provide the function of visualizing activation map within the current toolbox. One limitation is the rendered activation map is only in cortical level, however, since the application of depth electrodes, it will be interesting to visualize neural activities from the subcortical regions or structures. By taking advantages of the functions we offered within the toolbox (Sec. 3 and 4), we can also color the subcortical activation areas directly on each corresponding MRI slices for depth electrodes in the future, which will help to produce a 3D neural activity map inside the entire brain volume as well as may help to study the functions of different subcortical regions. In addition to the interpolated activation maps, another approach of enriching activation data visualization is plotting electrodes with different activation values (e.g., represented by different electrode diameter or color), which can give a direct sense of neural activation distribution across the brain volume. In spite of the needs for visualizing activation map using single neuroimaging modality, cross-modality studies also ask for the visualization of neural activity from multiple neuroimaging data for cross validation. A function that proposed in a recent versatile toolbox iELVis (Groppe et al., 2017), presenting multimodal overlay in the same brain, may act as a solution for addressing this need. In further step, we will add these new introduced features into current toolbox to provide users additional advantages towards visualization for iEEG related studies.

Besides, this toolbox has been developed to promote convenience and efficiency for the localization, but it still has space for improvements in terms of operation. First, it is designed for Mac system currently, thus this may restrict the wide usage of the toolbox. Therefore, making it compatible with more operating system in the next step is necessary in order to serve the scientific community widely. Second, during the visual inspection of anatomical label for each electrode (Sec. 3), we provide the operation on 2D slices under three different views instead of manipulating in 3D view directly. Although 2D view operation can fulfill the basic needs, providing the function of manipulation in 3D view is generally more intrinsic and convenient for users during operation (Branco et al., 2018a; Blenkmann et al., 2017). Third, Freesurfer is used in this toolbox. Even though we have integrated the dependent third-party software into one Matlab interface using command lines, developing a toolbox that is fully independent from any third-party software will gain significant convenience for users and thus deserves to be tried in the future.

Finally, iEEGview provides functions mainly for intracranial electrodes localization and visualization, while as another aspect of iEEG studies, signal processing and analysis for iEEG recordings is also of considerable importance. To address this need, some public software packages, such as EEGLAB (Delorme and Makeig, 2004), Brainstorm (Tadel et al., 2011), Fieldtrip (Oostenveld et al., 2011) and eConnectome (He et al., 2011), provide plentiful and useful functions for processing and analysis of electrophysiological data. For the iEEGview package, once the localization of electrodes was completed, with the proper processing of recorded signals, it is easily extensible for visualizing purpose of certain iEEG related studies, such as epileptic seizure onset detection (Bartolomei et al., 2008), functional mapping (Brunner et al., 2009; Trebuchon and Chauvel, 2016) and 3D brain connectivity network (Brovelli et al., 2017; Ter Wal et al., 2018). Hence, to better serve the research and clinical community, it is worth the efforts of building additional signal processing and

analyzing module in the future. The authors also welcome field researchers to make contributions to this software together.

7. Conclusions

In the present work, we introduce a multifunction toolbox, iEEGview, for the localization and visualization of human intracranial electrodes. To our best knowledge, iEEGview is the first public Matlab toolbox that integrates introduced prominent features together, including: 1) localizing depth and subdural electrodes (or the combination) with brain shift correction; 2) identifying the anatomical label of each electrode, providing additional visual inspection function and computing degree of confidence in assigning an anatomical label for each depth electrode contact; 3) supporting activation map generation; 4) offering methods for mapping two type of electrodes (i.e., depth and subdural) from native brain space into common brain space; 5) providing GUI based operation, from where users can run the full localization pipeline with low dependence on third-party software. In summary, iEEGview holds integrated capabilities for intracranial electrodes localization and visualization, offers simplicity and reliability in terms of operation, and provides solutions for addressing raised technical challenges that existed in this field. Consequently, iEEGview may serve as an effective and practical tool in promoting human iEEG studies.

Supplementary Material

Refer to Web version on PubMed Central for supplementary material.

Acknowledgments

This work was supported by grants from the NIH/NIBIB (P41-EB018783, R01-EB026439), the NIH/NINDS (U01-NS108916 and U24-NS109103), the NIH/NIMH (P50-MH109429), Fondazione Neurone, the National Natural Science Foundation of China (No. 91848112, No. 61761166006), the Shanghai Municipal Commission of Health and Family Planning (No. 2017ZZ01006), the Natural Science Foundation and Major Basic Research Program of Shanghai (No. 16JC1420102) and the Shanghai Municipal Science and Technology Major Project (No. 2018SHZDZX03). The software package is freely available through the link (https://github.com/GuangyeLiGit/iEEGview.git).

Appendix

Appendix A. Abbreviations

Alphabetical list of abbreviations used in this paper.

CRS	Column-Row-Slice
CT	Computerized Tomography
ECoG	Electrocorticography
fMRI	functional Magnetic Resonance Imaging
GUI	Graph User Interface
iEEG	intracranial Electroencephalography

MNI	Montreal Neurological Institute
MRI	Magnetic Resonance Imaging
PTD	Proximal Tissue Density
RAS	Right-Anterior-Superior
ROI	Region of Interest
SEEG	Stereo-Electroencephalography
SPM	Statistical Parametric Mapping

Appendix

8. Appendix B. Supplementary Material

A demonstration video of iEEGview is shown in Sec. 8

References

Arnal LH, Kleinschmidt A, Spinelli L, Giraud AL, Megevand P, 2019 The rough sound of salience enhances aversion through neural synchronisation. Nat Commun 10 (1), 3671. [PubMed: 31413319]

Arnulfo G, Hirvonen J, Nobili L, Palva S, Palva JM, 2015a Phase and amplitude correlations in resting-state activity in human stereotactical EEG recordings. Neuroimage 112, 114–27. [PubMed: 25721426]

Arnulfo G, Narizzano M, Cardinale F, Fato MM, Palva JM, 2015b Automatic segmentation of deep intracerebral electrodes in computed tomography scans. BMC Bioinformatics 16 (1), 99. [PubMed: 25887573]

Ashburner J, Friston KJ, 1999 Nonlinear spatial normalization using basis functions. Hum Brain Mapp 7 (4), 254–266. [PubMed: 10408769]

Avanzini P, Abdollahi RO, Sartori I, Caruana F, Pelliccia V, Casaceli G, Mai R, Lo Russo G, Rizzolatti G, Orban GA, 2016 Four-dimensional maps of the human somatosensory system. Proc Natl Acad Sci U S A 113 (13), E1936–43. [PubMed: 26976579]

Ayoubian L, Lacoma H, Gotman J, 2010 Automatic seizure detection in SEEG using high frequency activities in wavelet domain. Med Eng Phys 35 (3), 319–328.

Azarion AA, Wu J, Pearce A, Krish VT, Wagenaar J, Chen W, Zheng Y, Wang H, Lucas TH, Litt B, Gee JC, Davis KA, 2014 An open-source automated platform for three-dimensional visualization of subdural electrodes using CT-MRI coregistration. Epilepsia 55 (12), 2028–2037. [PubMed: 25377267]

Bartolomei F, Chauvel P, Wendling F, 2008. Epileptogenicity of brain structures in human temporal lobe epilepsy: a quantified study from intracerebral EEG. Brain 131 (Pt 7), 1818–30. [PubMed: 18556663]

Bartolomei F, Nica A, Valenti-Hirsch MP, Adam C, Denuelle M, 2018 Interpretation of SEEG recordings. Neurophysiol Clin 48 (1), 53–57. [PubMed: 29289423]

Behncke J, Kern M, Ruescher J, Schulze-Bonhage A, Ball T, 2019 Probabilistic neuroanatomical assignment of intracranial electrodes using the ELAS toolbox. J Neurosci Methods 327, 108396.

Behrens E, Zentner J, van Roost D, Hufnagel A, Elger CE, Schramm J, 1994 Subdural and depth electrodes in the presurgical evaluation of epilepsy. Acta Neurochirurgica 128 (1), 84–87. [PubMed: 7847148]

Betzel RF, Medaglia JD, Kahn AE, Soffer J, Schonhaut DR, Bassett DS, 2019 Structural, geometric and genetic factors predict interregional brain connectivity patterns probed by electrocorticography. Nat Biomed Eng.

Bhavaraju NC, Nagaraddi V, Chetlapalli SR, Osorio I, 2002 Electrical and thermal behavior of non-ferrous noble metal electrodes exposed to MRI fields. Magn Reson Imaging 20 (4), 351–357. [PubMed: 12165354]

Blenkmann AO, Phillips HN, Princich JP, Rowe JB, Bekinschtein TA, Muravchik CH, Kochen S, 2017 iElectrodes: A comprehensive open-source toolbox for depth and subdural grid electrode localization. Front Neuroinform 11, 14. [PubMed: 28303098]

Branco MP, Gaglianese A, Glen DR, Hermes D, Saad ZS, Petridou N, Ramsey NF, 2018a ALICE: A tool for automatic localization of intra-cranial electrodes for clinical and high-density grids. J Neurosci Methods 301, 43–51. [PubMed: 29100838]

Branco MP, Leibbrand M, Vansteensel MJ, Freudenburg ZV, Ramsey NF, 2018b GridLoc: An automatic and unsupervised localization method for high-density ECoG grids. Neuroimage 179, 225–234. [PubMed: 29920373]

Britton JW, 2018 Electrical stimulation mapping with stereo-EEG electrodes. J Clin Neurophysiol 35 (2), 110–114. [PubMed: 29499018]

Brovelli A, Badier JM, Bonini F, Bartolomei F, Coulon O, Auzias G, 2017 Dynamic reconfiguration of visuomotor-related functional connectivity networks. J Neurosci 37 (4), 839–853. [PubMed: 28123020]

Brunner P, Ritaccio AL, Lynch TM, Emrich JF, Wilson JA, Williams JC, Aarnoutse EJ, Ramsey NF, Leuthardt EC, Bischof H, Schalk G, 2009 A practical procedure for real-time functional mapping of eloquent cortex using electrocorticographic signals in humans. Epilepsy Behav 15 (3), 278–86. [PubMed: 19366638]

Cardinale F, Gonzalez-Martinez J, Lo Russo G, 2016 SEEG, happy anniversary! World Neurosurg 85, 1–2. [PubMed: 26679262]

Collins DL, Neelin P, Peters TM, Evans AC, 1994 Automatic 3D intersubject registration of MR volumetric data in standardized Talairach space. J Comput Assist Tomo 18 (2), 192–205.

Conner CR, Chen G, Pieters TA, Tandon N, 2014 Category specific spatial dissociations of parallel processes underlying visual naming. Cereb Cortex 24 (10), 2741–50. [PubMed: 23696279]

Coon WG, Gunduz A, Brunner P, Ritaccio AL, Pesaran B, Schalk G, 2016 Oscillatory phase modulates the timing of neuronal activations and resulting behavior. Neuroimage 133, 294–301. [PubMed: 26975551]

Coon WG, Schalk G, 2016 A method to establish the spatiotemporal evolution of task-related cortical activity from electrocorticographic signals in single trials. J Neurosci Methods 271, 76–85. [PubMed: 27427301]

Crone NE, Sinai A, Korzeniewska A, 2006 High-frequency gamma oscillations and human brain mapping with electrocorticography. Vol. 159 Elsevier, pp. 275–295.

Dalal SS, Edwards E, Kirsch HE, Barbaro NM, Knight RT, Nagarajan SS, 2008 Localization of neurosurgically implanted electrodes via photographMRIradiograph coregistration. J Neurosci Methods 174 (1), 106–115. [PubMed: 18657573]

de Pesters A, Coon WG, Brunner P, Gunduz A, Ritaccio AL, Brunet NM, de Weerd P, Roberts MJ, Oostenveld R, Fries P, Schalk G, 2016 Alpha power indexes task-related networks on large and small scales: A multimodal ECoG study in humans and a non-human primate. Neuroimage 134, 122–131. [PubMed: 27057960]

Delorme A, Makeig S, 2004 EEGLAB: an open source toolbox for analysis of single-trial EEG dynamics including independent component analysis. J Neurosci Methods 134 (1), 9–21. [PubMed: 15102499]

Desikan RS, Segonne F, Fischl B, Quinn BT, Dickerson BC, Blacker D, Buckner RL, Dale AM, Maguire RP, Hyman BT, Albert MS, Killiany RJ, 2006 An automated labeling system for subdividing the human cerebral cortex on MRI scans into gyral based regions of interest. Neuroimage 31 (3), 968–80. [PubMed: 16530430]

Destrieux C, Fischl B, Dale AM, Halgren E, 2009 A sulcal depth-based anatomical parcellation of the cerebral cortex. Neuroimage 47, S151.

Dykstra AR, Chan AM, Quinn BT, Zepeda R, Keller CJ, Cormier J, Madsen JR, Eskandar EN, Cash SS, 2012 Individualized localization and cortical surface-based registration of intracranial electrodes. Neuroimage 59 (4), 3563–70. [PubMed: 22155045]

Elias WJ, Fu K-M, Frysinger RC, 2007 Cortical and subcortical brain shift during stereotactic procedures. J Neurosurg 107 (5), 983–988. [PubMed: 17977271]

Enatsu R, Bulacio J, Najm I, Wyllie E, So NK, Nair DR, Foldvary-Schaefer N, Bingaman W, Gonzalez-Martinez J, 2014 Combining stereo-electroencephalography and subdural electrodes in the diagnosis and treatment of medically intractable epilepsy. J Clin Neurosci 21 (8), 1441–5. [PubMed: 24650680]

Evans AC, Janke AL, Collins DL, Baillet S, 2012 Brain templates and atlases. Neuroimage 62 (2), 911–22. [PubMed: 22248580]

Fischl B, 2004 Automatically parcellating the human cerebral cortex. Cerebral Cortex 14 (1), 11–22. [PubMed: 14654453]

Fischl B, Salat DH, Busa E, Albert M, Dieterich M, Haselgrove C, van der Kouwe A, Killiany R, Kennedy D, Klaveness S, Montillo A, Makris N, Rosen B, Dale AM, 2002 Whole brain segmentation. Neuron 33 (3), 341–355. [PubMed: 11832223]

Fischl B, Sereno MI, Tootell RB, Dale AM, 1999 High-resolution intersubject averaging and a coordinate system for the cortical surface. Hum Brain Mapp 8 (4), 272–284. [PubMed: 10619420]

Gonzalez-Martinez J, Mullin J, Vadera S, Bulacio J, Hughes G, Jones S, Enatsu R, Najm I, 2014 Stereotactic placement of depth electrodes in medically intractable epilepsy. J Neurosurg 120 (3), 639–644. [PubMed: 24405074]

Groppe DM, Bickel S, Dykstra AR, Wang X, Megevand P, Mercier MR, Lado FA, Mehta AD, Honey CJ, 2017 iELVis: An open source MATLAB toolbox for localizing and visualizing human intracranial electrode data. J Neurosci Methods 281, 40–48. [PubMed: 28192130]

Guevara M, Roman C, Houenou J, Duclap D, Poupon C, Mangin JF, Guevara P, 2017 Reproducibility of superficial white matter tracts using diffusion-weighted imaging tractography. Neuroimage 147, 703–725. [PubMed: 28034765]

Hastreiter P, Rezk-Salama C, Soza G, Bauer M, Greiner G, Fahlbusch R, Ganslandt O, Nimsky C, 2004 Strategies for brain shift evaluation. Med Image Anal 8 (4), 447–464. [PubMed: 15567708]

He B, Dai Y, Astolfi L, Babiloni F, Yuan H, Yang L, 2011 econnectome: A matlab toolbox for mapping and imaging of brain functional connectivity. J Neurosci Methods 195 (2), 261–9. [PubMed: 21130115]

Hermes D, Miller KJ, Noordmans HJ, Vansteensel MJ, Ramsey NF, 2010 Automated electrocorticographic electrode localization on individually rendered brain surfaces. J Neurosci Methods 185 (2), 293–8. [PubMed: 19836416]

Holmes CJ, Hoge R, Collins L, Woods R, Toga AW, Evans AC, 1998 Enhancement of MR images using registration for signal averaging. J Comput Assist Tomo 22 (2), 324–333.

Jenkinson M, Smith S, 2001 A global optimisation method for robust affine registration of brain images. Med Image Anal 5 (2), 143–156. [PubMed: 11516708]

Klein A, Tourville J, 2012 101 labeled brain images and a consistent human cortical labeling protocol. Front Neurosci 6, 171. [PubMed: 23227001]

Koessler L, Benar C, Maillard L, Badier J-M, Vignal JP, Bartolomei F, Chauvel P, Gavaret M, 2010 Source localization of ictal epileptic activity investigated by high resolution EEG and validated by SEEG. Neuroimage 51 (2), 642–653. [PubMed: 20206700]

Kovalev D, Spreer J, Honegger J, Zentner J, Schulze-Bonhage A, Huppertz H-J, 2005 Rapid and fully automated visualization of subdural electrodes in the presurgical evaluation of epilepsy patients. Am J Neuroradiol 26 (5), 1078. [PubMed: 15891163]

Kubanek J, Miller KJ, Ojemann JG, Wolpaw JR, Schalk G, 2009 Decoding flexion of individual fingers using electrocorticographic signals in humans. J Neural Eng 6 (6), 066001. [PubMed: 19794237]

Kubanek J, Schalk G, 2015 NeuralAct: A tool to visualize electrocortical (ECoG) activity on a three-dimensional model of the cortex. Neuroinformatics 13 (2), 167–74. [PubMed: 25381641]

Lachaux JP, Rudrauf D, Kahane P, 2003 Intracranial EEG and human brain mapping. J Physiol-Paris 97 (4), 613–628. [PubMed: 15242670]

Landre E, Chipaux M, Maillard L, Szurhaj W, Trebuchon A, 2018 Electrophysiological technical procedures. Neurophysiol Clin 48 (1), 47–52. [PubMed: 29254834]

Leuthardt EC, Schalk G, Wolpaw JR, Ojemann JG, Moran DW, 2004 A brain-computer interface using electrocorticographic signals in humans. J Neural Eng 1 (2), 63–71. [PubMed: 15876624]

Li G, Jiang S, Paraskevopoulou SE, Wang M, Xu Y, Wu Z, Chen L, Zhang D, Schalk G, 2018a Optimal referencing for stereo-electroencephalographic (SEEG) recordings. Neuroimage 183, 327–335. [PubMed: 30121338]

Li G, Jiang S, Wang M, Wu Z, Brunner P, Schalk G, Chen L, Zhang D, 2018b SEEGview: A toolbox for localization and visualization of stereoelectroencephalography (SEEG) electrodes. In: 2018 IEEE International Conference on Systems, Man, and Cybernetics (SMC) pp. 67–70.

Li G, Jiang S, Xu Y, Wu Z, Chen L, Zhang D, 2017 A preliminary study towards prosthetic hand control using human stereo-electroencephalography (SEEG) signals. In: 2017 8th International IEEE/EMBS Conference on Neural Engineering (NER) pp. 375–378.

Mazziotta JC, Toga AW, Evans A, Fox P, Lancaster J, 1995 A probabilistic atlas of the human brain: theory and rationale for its development. Neuroimage 2 (2), 89–101. [PubMed: 9343592]

Medina Villalon S, Paz R, Roehri N, Lagarde S, Pizzo F, Colombet B, Bartolomei F, Carron R, Benar CG, 2018 EpiTools, A software suite for presurgical brain mapping in epilepsy: Intracerebral EEG. J Neurosci Methods 303, 7–15. [PubMed: 29605667]

Mercier MR, Bickel S, Megevand P, Groppe DM, Schroeder CE, Mehta AD, Lado FA, 2017 Evaluation of cortical local field potential diffusion in stereotactic electro-encephalography recordings: A glimpse on white matter signal. Neuroimage 147, 219–232. [PubMed: 27554533]

Miller KJ, Makeig S, Hebb AO, Rao RPN, denNijs M, Ojemann JG, 2007 Cortical electrode localization from X-rays and simple mapping for electrocorticographic research: The Location on Cortex (LOC) package for MATLAB. J Neurosci Methods 162 (1), 303–308. [PubMed: 17343918]

Miller KJ, Schalk G, Fetz EE, den Nijs M, Ojemann JG, Rao RPN, 2010 Cortical activity during motor execution, motor imagery, and imagery-based online feedback. Proc Natl Acad Sci U S A 107 (9), 4430. [PubMed: 20160084]

Moré JJ, 1978 The Levenberg-Marquardt algorithm: implementation and theory. Springer, pp. 105–116.

Murphy BA, Miller JP, Gunalan K, Ajiboye AB, 2016 Contributions of subsurface cortical modulations to discrimination of executed and imagined grasp forces through stereoelectroencephalography. PLoS ONE 11 (3), e0150359.

Narizzano M, Arnulfo G, Ricci S, Toselli B, Tisdall M, Canessa A, Fato MM, Cardinale F, 2017 SEEG assistant: a 3DSlicer extension to support epilepsy surgery. BMC Bioinformatics 18 (1), 124. [PubMed: 28231759]

Nourski KV, Steinschneider M, Rhone AE, Kawasaki H, Howard MA, r., Banks MI, 2018 Processing of auditory novelty across the cortical hierarchy: An intracranial electrophysiology study. Neuroimage 183, 412–424. [PubMed: 30114466]

Oostenveld R, Fries P, Maris E, Schoffelen J-M, 2011 FieldTrip: open source software for advanced analysis of MEG, EEG, and invasive electrophysiological data. Comput Intell Neurosci 2011, 1. [PubMed: 21837235]

Parvizi J, Kastner S, 2018 Promises and limitations of human intracranial electroencephalography. Nat Neurosci 21 (4), 474–483. [PubMed: 29507407]

Penny WD, Friston KJ, Ashburner JT, Kiebel SJ, Nichols TE, 2011 Statistical Parametric Mapping: The Analysis of Functional Brain Images. Elsevier Science.

Pieters TA, Conner CR, Tandon N, 2013 Recursive grid partitioning on a cortical surface model: an optimized technique for the localization of implanted subdural electrodes. J Neurosurg 118 (5), 1086–1097. [PubMed: 23495883]

Posner M, Szczepanski SM, Crone NE, Kuperman RA, Auguste KI, Parvizi J, Knight RT, 2014 Dynamic changes in phase-amplitude coupling facilitate spatial attention control in fronto-parietal cortex. PLoS Biology 12 (8), e1001936.

Princich JP, Wassermann D, Latini F, Oddo S, Blenkmann AO, Seifer G, Kochen S, 2013 Rapid and efficient localization of depth electrodes and cortical labeling using free and open source medical software in epilepsy surgery candidates. Front Neurosci 7, 260. [PubMed: 24427112]

Roberts DW, Miga MI, Hartov A, Kennedy FE, Paulsen KD, 1998 Intraoperative brain shift and deformation: A quantitative analysis of cortical displacement in 28 cases. Neurosurgery 43 (4), 749–758. [PubMed: 9766300]

Salat DH, Lee SY, van der Kouwe AJ, Greve DN, Fischl B, Rosas HD, 2009 Age-associated alterations in cortical gray and white matter signal intensity and gray to white matter contrast. Neuroimage 48 (1), 21–8. [PubMed: 19580876]

Sani OG, Yang Y, Lee MB, Dawes HE, Chang EF, Shanechi MM, 2018 Mood variations decoded from multi-site intracranial human brain activity. Nat Biotechnol 36 (10), 954–961. [PubMed: 30199076]

Schaer M, Cuadra MB, Tamarit L, Lazeyras F, Eliez S, Thiran JP, 2008 A surface-based approach to quantify local cortical gyrification. IEEE Trans Med Imaging 27 (2), 161–70. [PubMed: 18334438]

Schalk G, Kapeller C, Guger C, Ogawa H, Hiroshima S, Lafer-Sousa R, Saygin ZM, Kamada K, Kanwisher N, 2017a Facephenes and rainbows: Causal evidence for functional and anatomical specificity of face and color processing in the human brain. Proc Natl Acad Sci U S A.

Schalk G, Kubanek J, Miller KJ, Anderson NR, Leuthardt EC, Ojemann JG, Limbrick D, Moran D, Gerhardt LA, Wolpaw JR, 2007 Decoding twodimensional movement trajectories using electrocorticographic signals in humans. J Neural Eng 4 (3), 264–75. [PubMed: 17873429]

Schalk G, Marple J, Knight RT, Coon WG, 2017b Instantaneous voltage as an alternative to power- and phase-based interpretation of oscillatory brain activity. Neuroimage 157, 545–554. [PubMed: 28624646]

Stolk A, Griffin S, van der Meij R, Dewar C, Saez I, Lin JJ, Piantoni G, Schoffelen JM, Knight RT, Oostenveld R, 2018 Integrated analysis of anatomical and electrophysiological human intracranial data. Nat Protoc 13 (7), 1699–1723. [PubMed: 29988107]

Studholme C, Hawkes DJ, Hill DL, 1998 Normalized entropy measure for multimodality image alignment. In: Medical Imaging 1998: Image Processing. Vol. 3338 pp. 132–143.

Surbeck W, Bouthillier A, Weil AG, Crevier L, Carmant L, Lortie A, Major P, Nguyen DK, 2011 The combination of subdural and depth electrodes for intracranial EEG investigation of suspected insular (perisylvian) epilepsy. Epilepsia 52 (3), 458–466. [PubMed: 21204825]

Sweet JA, Hdeib AM, Sloan A, Miller JP, 2013 Depths and grids in brain tumors: implantation strategies, techniques, and complications. Epilepsia 54 Suppl 9, 66–71.

Swift JR, Coon WG, Guger C, Brunner P, Bunch M, Lynch T, Frawley B, Ritaccio AL, Schalk G, 2018 Passive functional mapping of receptive language areas using electrocorticographic signals. Clin Neurophysiol 129 (12), 2517–2524. [PubMed: 30342252]

Tadel F, Baillet S, Mosher JC, Pantazis D, Leahy RM, 2011 Brainstorm: a user-friendly application for MEG/EEG analysis. Comput Intel Neurosc 2011, 8.

Taimouri V, Akhondi-Asl A, Tomas-Fernandez X, Peters JM, Prabhu SP, Poduri A, Takeoka M, Loddenkemper T, Bergin AM, Harini C, Madsen JR, Warfield SK, 2014 Electrode localization for planning surgical resection of the epileptogenic zone in pediatric epilepsy. Int J Comput Assist Radiol Surg 9 (1), 91–105. [PubMed: 23793723]

Ter Wal M, Cardellicchio P, LoRusso G, Pelliccia V, Avanzini P, Orban GA, Tiesinga PHE, 2018 Characterization of network structure in stereoEEG data using consensus-based partial coherence. Neuroimage 179, 385–402. [PubMed: 29885486]

Trebuchon A, Chauvel P, 2016 Electrical stimulation for seizure induction and functional mapping in stereoelectroencephalography. J Clin Neurophysiol 33 (6), 511–521. [PubMed: 27918346]

van Rooijen BD, Backes WH, Schijns OE, Colon A, Hofman PA, 2013 Brain imaging in chronic epilepsy patients after depth electrode (stereoelectroencephalography) implantation: magnetic resonance imaging or computed tomography? Neurosurgery 73 (3), 543–9. [PubMed: 23719051]

Wu J, Ngo GH, Greve D, Li J, He T, Fischl B, Eickhoff SB, Yeo BT, 2018 Accurate nonlinear mapping between MNI volumetric and FreeSurfer surface coordinate systems. Hum Brain Mapp 39 (9), 3793–3808. [PubMed: 29770530]

Yang AI, Wang X, Doyle WK, Halgren E, Carlson C, Belcher TL, Cash SS, Devinsky O, Thesen T, 2012 Localization of dense intracranial electrode arrays using magnetic resonance imaging. Neuroimage 63 (1), 157–165. [PubMed: 22759995]

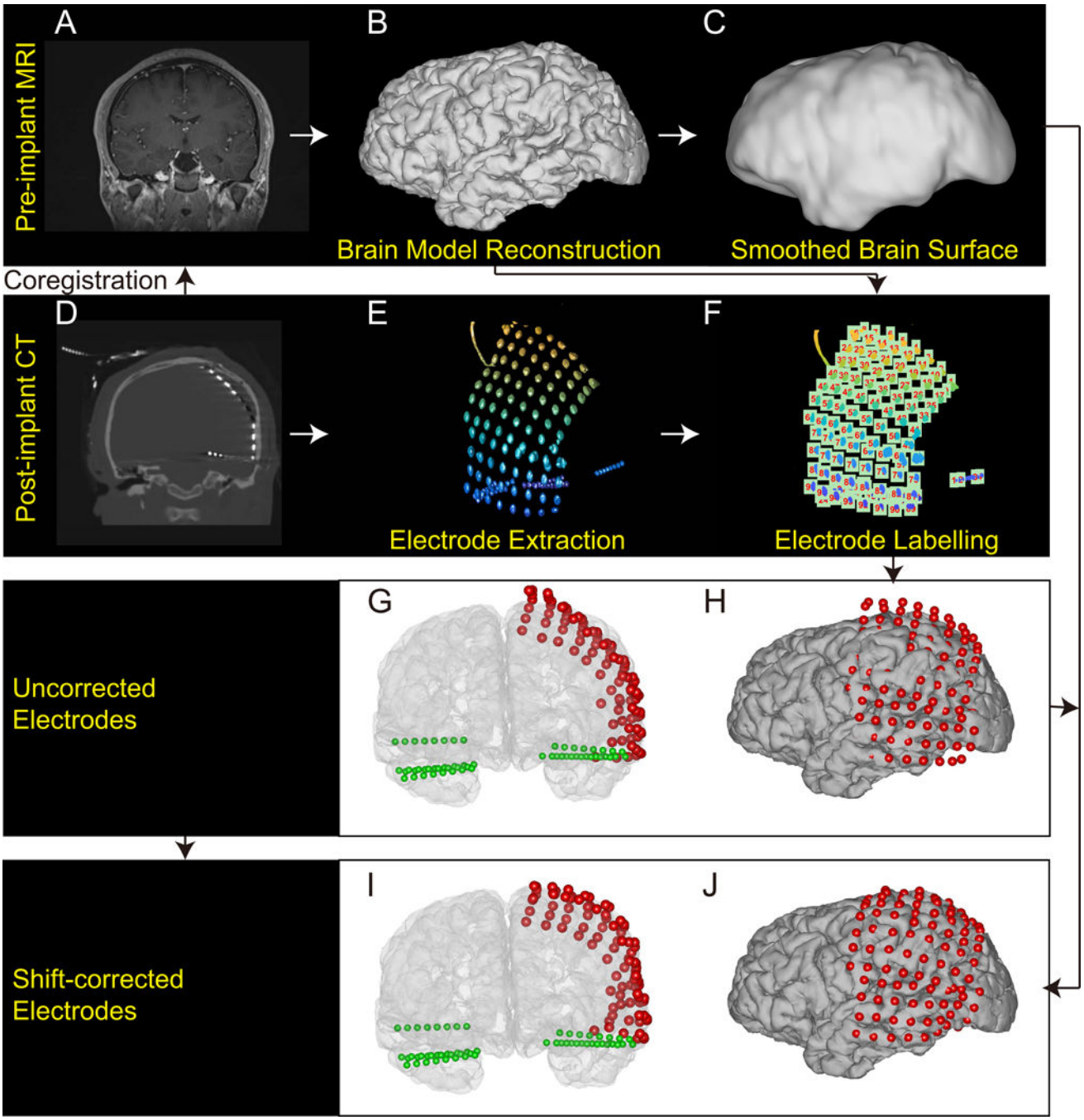

Figure 1.

Electrode localization process of the toolbox.**A)** Pre-implant MRI images from a single subject. **B)** The brain reconstruction results using the MRI images from A. The brain segmentation results are generated after the brain reconstruction. **C)** The smoothed brain surface generated after B. This process is implemented automatically by executing Freesurfer functions from the toolbox. **D)** Post-implant CT images are aligned to the MRI images by running the coregistration function from the toolbox. **E)** Location and profiles of all implanted electrodes are extracted from the coregistered CT images. **F)** Electrode

labelling process after electrode extraction. Coordinates of all the electrodes are computed and transformed into the space where the individual brain (B,C) is located after this step in the toolbox. **G/H)** Original reconstructed brain surface and electrodes before brain shift correction. **I/J)** Reconstructed brain surface and electrodes after brain shift correction. Subject information from Subject 28 are used here for illustration.

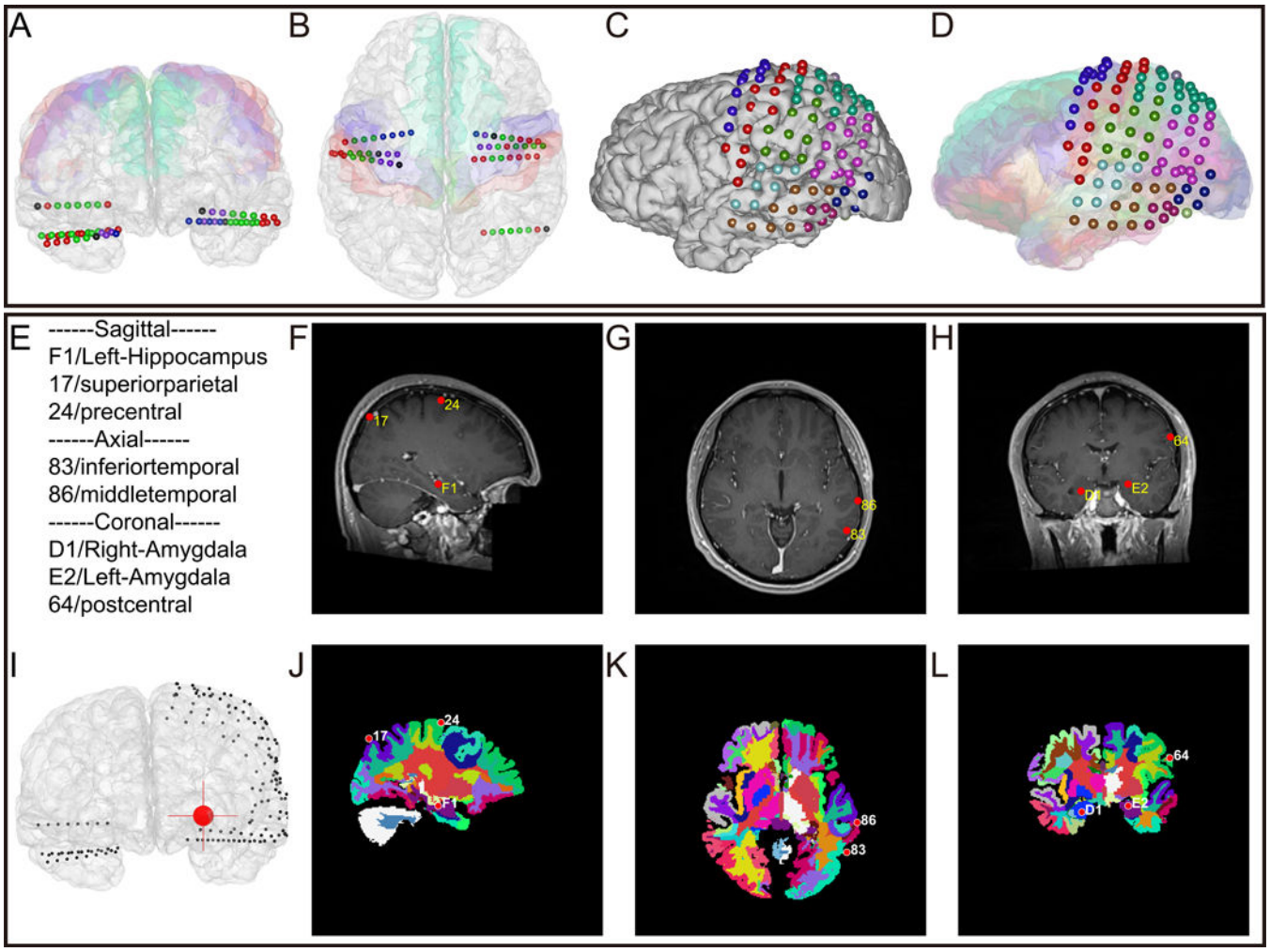

Figure 2.

Illustration of the anatomical information identification function of the toolbox. **A/B)** Coronal/axial view of identified anatomical information for depth electrodes and individual brain. Depth electrode contacts are colored differently to represent different anatomical locations: red for gray matter, green for white matter, purple for hippocampus, blue for amygdala, black for unknown areas. The different colours on cortical surface indicate different cortical regions. The toolbox enables the coloring of specified cortical regions based on needs. **C/D)** Illustration of anatomical identification for subdural electrodes without/with presenting cortical parcellation results (colorful cortex). Anatomical location for each electrode is shown in the same color as the segmented cortical region where the electrode is located. For A-D, Desikan-Killiany atlas is used here for visualization purpose. **E-L)** The graph user interface (GUI) of iEEGview for the manual inspection of each electrode's anatomical location. Bars used for adjusting image slices are not shown in this figure for visualization purpose. See Supplementary Materials (Sec. 8) for more details. **E)** The automatically identified anatomical name of electrodes presented in F-H. **F/G/H)** Sagittal/axial/coronal view of electrodes and original MRI images. Electrodes are shown in red dots for each MRI slice if there exists. The name of each electrode is presented in

yellow. **I)** 3D view of the brain and electrodes. Red cross indicates the real-time coordinates of current image slices. **J/K/L)** Sagittal/axial/coronal view of electrodes and brain segmentation. Electrodes are shown in red dots for each atlas slice if there exists. Different colours in each slice represent different segmented brain regions. The name of each electrode is shown in white. White matter segmentation results are presented in the images as well. Subject information from Subject 28 are used here for illustration.

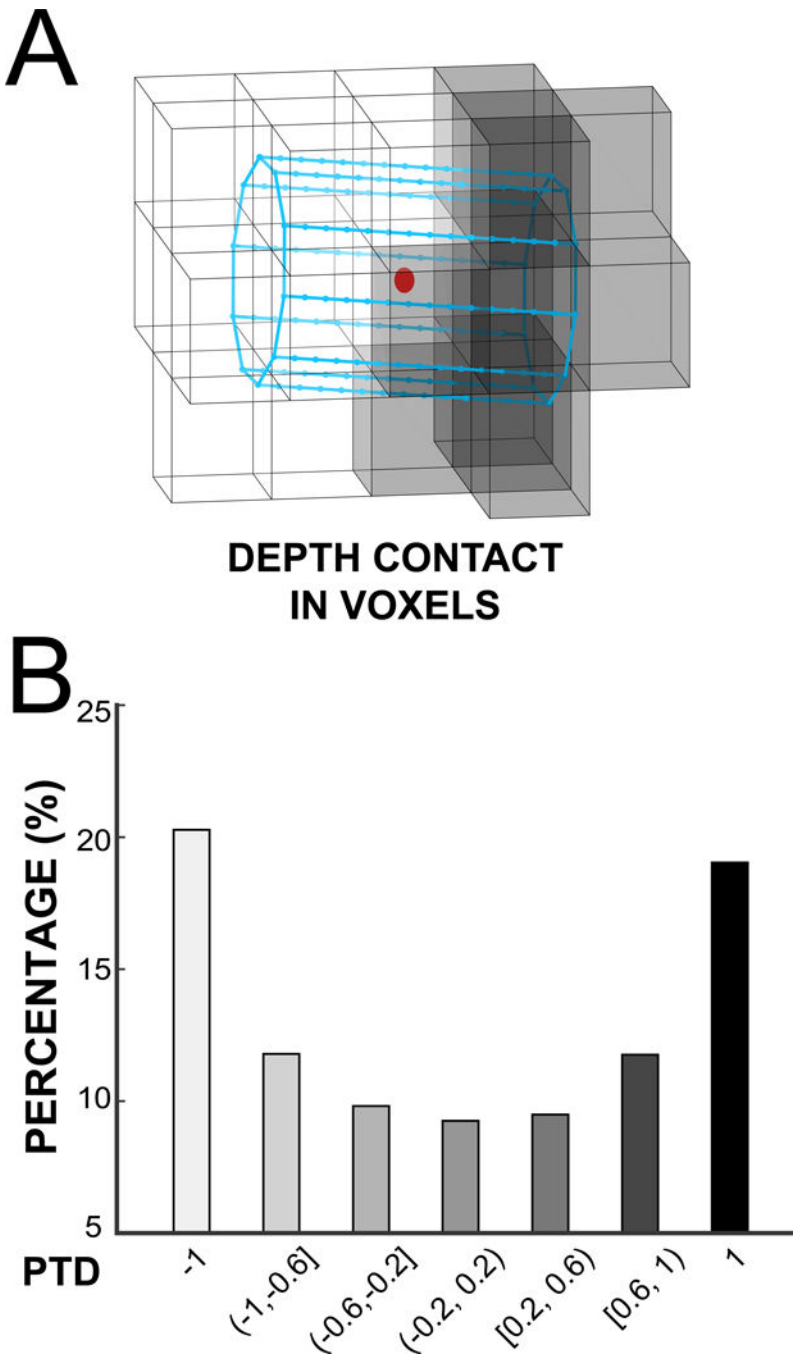

Figure 3.

Illustration of proximal tissue density (PTD) for depth electrode contacts. **A)** A schematic drawing of PTD algorithm for depth contacts. The augmented contact (light blue lines, red dot represents the contact centroid) is surrounded by both gray matter (gray voxels) and white matter (white voxels). Each voxel is 1×1×1 mm^3. The number of gray and white matter voxels are used for PTD calculation. **B)** PTD distribution across 23 human subjects (3158 depth contacts). Bins of PTD value are shown in x-axis. The percentage value is calculated by dividing the number of contacts found within each bin by the total number of

depth contacts across all subjects. PTD value of depth contacts that are not located in gray matter or white matter (e.g., deep subcortical structures) are not displayed.

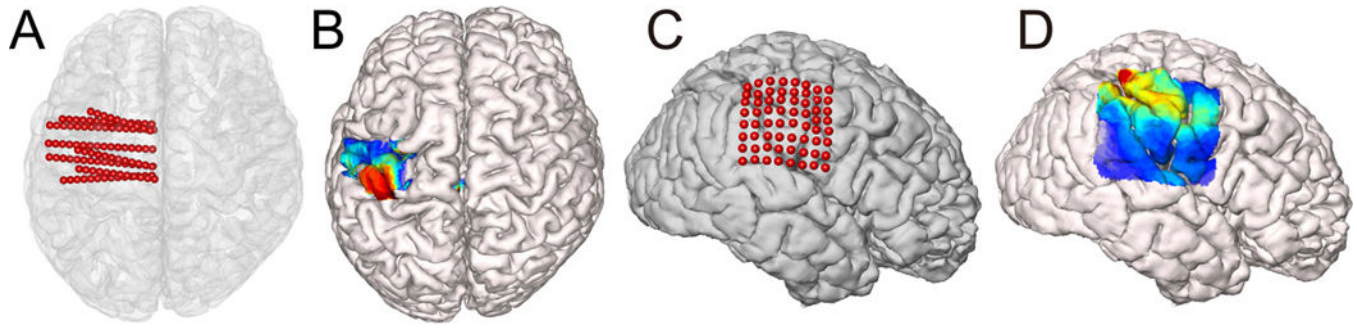

Figure 4.

Illustration of activation map for depth and subdural electrodes respectively. **A)** Locations of depth electrode contacts (red) from a subject (Subject 22). **B)** The rendered activation map using the activation value from electrodes A under the default parameters (activation value is obtained from the subjects performing the task (Li et al., 2018a), Bonferroni correction of activation value is applied to the activation map). **C)** Locations of subdural electrodes (red) from a subject (Subject 23). **D)** The rendered activation map using a random activation value from electrodes C under the default parameters.

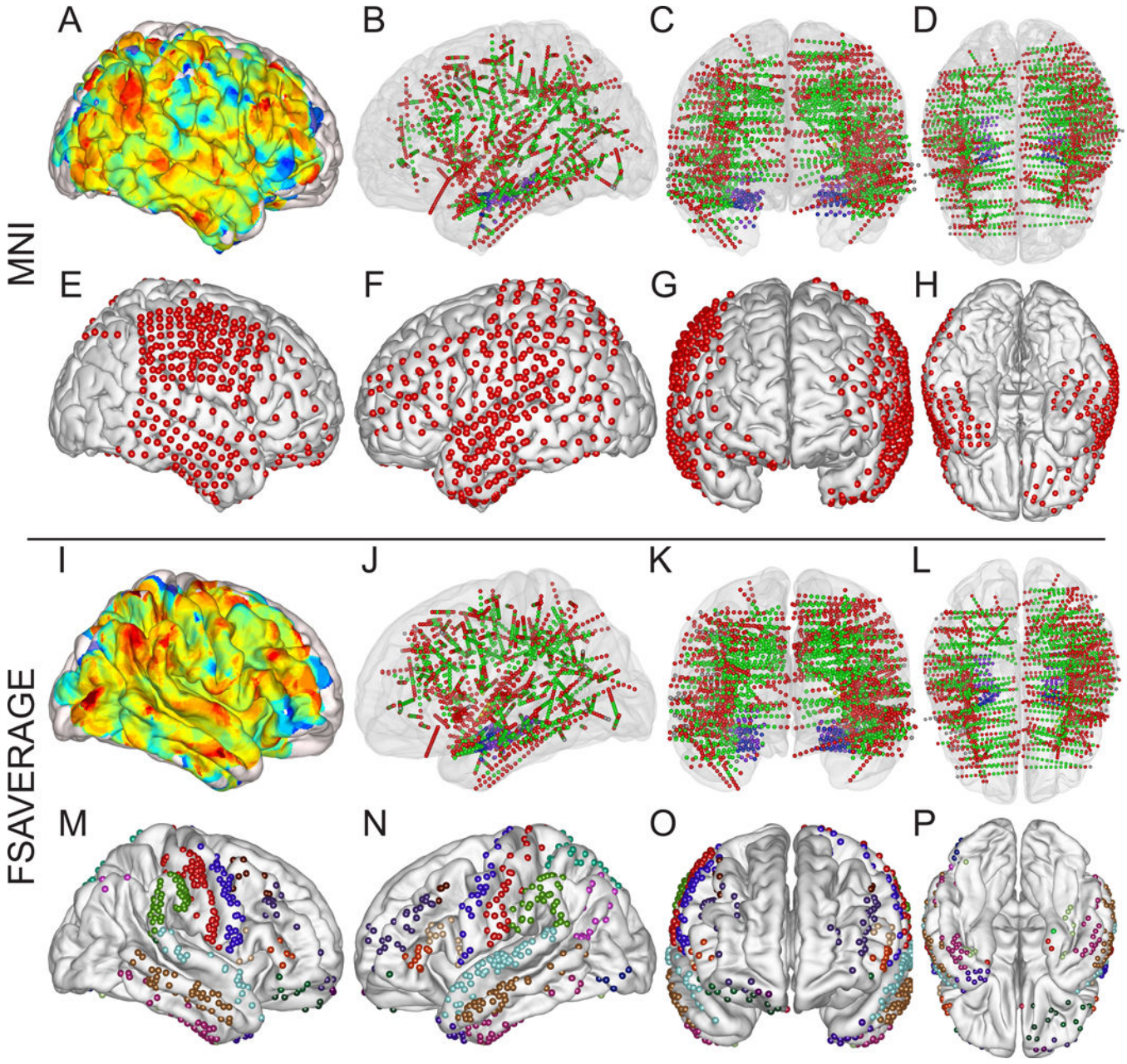

Figure 5.

Illustration of mapping into standard brain function for depth electrodes and subdural electrodes. **A)** Activation map generated on the Montreal Neurological Institute (MNI) brain model using random activation value from all depth electrodes. All the depth electrodes (B-D) are first projected into the right hemisphere for the rendering of activation map for visualization purpose. **B/C/D)** Sagittal/coronal/axial view of all depth contacts projected into a MNI brain model using volumetric registration method from 23 subjects (Subject 1–22 and 28, n=3158). Contacts are shown with small balls. Different colours represent different anatomical locations, where red indicates gray matter, green indicates white matter, purple indicates hippocampus, blue indicates amygdala, yellow indicates putamen, and gray

indicates the remaining regions. **E/F/G/H)** Different views of all subdural electrodes projected onto a standard brain model (MNI) from 6 subjects (Subject 23–28, n=568). Each subdural electrode is represented with red balls. The subdural electrodes from individual subjects are transformed into the common brain space using volumetric registration method first and then projected onto the surface of the MNI brain model (Sec. 2). **I)** Activation map generated on the Freesurfer average brain model (FSAverage) using the same activation value with A from all depth electrodes. All the other configurations are the same with A. **J/K/L)** Sagittal/coronal/axial view of all depth contacts projected into the average brain model using linear space transformation from 23 subjects (Subject 1–22 and 28, n=3158). All the other configurations are the same with B-D. **E/F/G/H)** Different views of all subdural electrodes projected onto a standard brain model (FSAverage) using surface-based registration from 6 subjects (Subject 23–28, n=568). Electrodes are shown in different colors based on their anatomical locations. Desikan-Killiany atlas is used here for visualization purpose.